The Delayed Response of Airborne Thermometers: Part 2: Correcting for Dynamic Heating

William A. Cooper and others...

DRAFT March 2020

National Center for Atmospheric Research
Earth Observing Laboratory
Research Aviation Facility

Table of Contents

List of Figures

List of Tables

Preface and Abstract

In Part 1, the time response of some standard airborne thermometers was determined by observing the response to turbulent dynamic heating. For some standard airborne thermometers, the transfer function characterizing this time response was parameterized in terms of assumed differential equations or more generally via fitted expressions. In this paper, the consequences for how dynamic heating is treated are discussed. The standard processing approach used with most airborne measurement platforms is to determine the ambient or air temperature by subtracting a dynamic-heating correction from the measured recovery temperature. When the sensor cannot respond to fluctuations in dynamic heating, this procedure introduces errors and excess noise into the resulting air temperature. A modified correction procedure is proposed here that instead corrects for dynamic heating only after filtering to match the response of the temperature sensors. The filter used for this processing step is obtained from the transfer functions determined in Part 1. This has a beneficial effect on the variance spectra of temperature measurements.

Acknowledgments

This material is based upon work supported by the National Center for Atmospheric Research, which is a major facility sponsored by the National Science Foundation under Cooperative Agreement No. 1852977. Any opinions, findings and conclusions or recommendations expressed in this publication are those of the author(s) and do not necessarily reflect the views of the National Science Foundation. The data used in the examples presented are from the VOCALS (VAMOS Ocean-Cloud-Atmosphere-Land Study), SOCRATES (Southern Ocean Clouds, Radiation, Aerosol Transport Experimental Study) and the CSET (Cloud Systems Evolution in the Trades) experiment, each described at this URL. Citations for the data sets are included in the references. Measurements (UCAR/NCAR - Earth Observing Laboratory [2011], UCAR/NCAR - Earth Observing Laboratory [2019], UCAR/NCAR - Earth Observing Laboratory [2018]) were collected by the project experiment teams, and flight operations and data acquisition and processing were performed by the Research Aviation Facility, Earth Observing Laboratory, National Center for Atmospheric Research (NCAR). The analyses reported here were mostly performed using R (R Core Team [2019]), with RStudio (RStudio [2009]) and knitr (Xie [2013, 2014]). Data files in netCDF format have been read and written using the R package "ncdf4"; cf. Pierce [2015]. Substantial use also was made of the "ggplot2" package (Wickham [2009]) for R, and some fits relied on the "nleqslv" package for R Hasselman [2018]. Extensive use was made of the "stats" package, part of Core R. Some of the numerical integrations used the Runge-Kutta function from the "rmutil" package (Swihart and Lindsey [2019]).

1 Introduction

1.1 Overview

This series of papers was introduced in Part 1, where it was indicated that the overarching goal of these papers is to improve capabilities to measure sensible-heat flux from research aircraft. Toward that goal, Part 1 characterized the measured quantity, the "recovery temperature," using a parameterized transfer function. That paper did not discuss the implications for the final measurement of ambient or air temperature, which requires a correction for the dynamic heating of the sensor. This second paper in the series treats that correction. It might seem that this is minor and could be incorporated into other parts, but the claim here is that this correction as applied by essentially all operators of research aircraft introduces errors and noise into the measurement that should be eliminated. Making this point therefore seems worth a separate discussion. Part 1 and this paper will establish the foundation for Part 3, where measuring the flux of sensible heat is discussed and the corrections developed in the first two parts are applied.

2 The Dynamic-Heating Correction

The dynamic-heating term is discussed for example by Bange et al. [2013] (cf. their Eq. 2.23) and also in the working document describing processing algorithms in use at the Research Aviation Facility, NCAR: "RAF Technical Report: Processing Algorithms". These sources express the dynamic-heating term Q as

$$Q = \alpha_r \frac{V^2}{2C_p} = T_r \left(\frac{\alpha_r M^2 R_a/(2C_v)}{1 + \alpha_r M^2 R_a/(2C_v)} \right) \tag{1}$$

where α_r is the "recovery factor" characterizing the extent to which the air is brought to rest relative to the sensor, V is the airspeed, C_p and C_v are respectively the specific heat of air at constant pressure and constant volume, T_r is the (true) recovery temperature expressed in absolute units, M the Mach number, and R_a the gas constant for air. The recovery factor is close to unity for the sensors discussed in this report. The dynamic-heating term can exceed 20°C at NCAR/NSF GV flight speeds, so the correction is large and fluctuations in this term are often the dominant source of variability in the recovery temperature. The recovery temperature is related to the air or ambient temperature T_a via

$$T_r = T_a + Q \tag{2}$$

2.1 Errors conventionally introduced

Normal data processing subtracts the dynamic-heating term Q from the measured recovery temperature to estimate the actual air temperature. However, the dynamic-heating term often varies rapidly in a turbulent wind field and produces rapid changes in the true recovery temperature to which the temperature sensor may not respond. In that case, applying the standard dynamic-heating correction introduces erroneous fluctuations in the estimated ambient temperature.

Figure 1 illustrates the problem. The measurements are from a region reasonably consistent with an inertial sub-range, where the slope of the temperature variance spectrum would be expected to be -5/3 (or -2/3 in this plot where the spectrum is weighted by the frequency). The measured spectrum (RTF1) has a steeper slope than this but that would be expected if the time response attenuates the signal at higher frequencies. However, the variance spectrum for the estimated ambient temperature (ATF1) appears to have a substantial amount of high-frequency contamination. This matches well the spectrum for dynamic heating, but if the sensor worked correctly the recovery-temperature spectrum should exceed that of the ambient temperature, as is the case around 0.1 to 0.5 Hz, so that the subtraction of dynamic heating would produce smaller variance in the measured ambient temperature.

Data processing should instead remove an estimate of how dynamic heating affects the sensor. The approach followed in this paper is therefore to use the transfer function determined in Part 1 (e.g., Fig. 1 in that paper) to characterize the response to dynamic heating so that only that response can be subtracted from the measurement. This is made

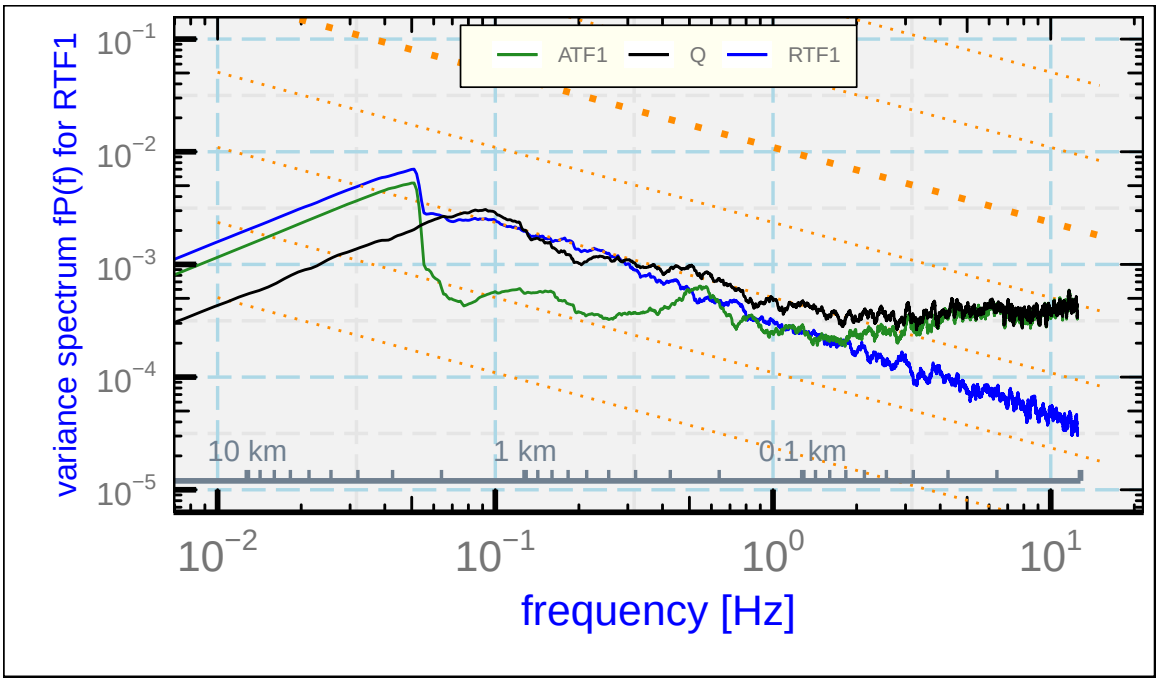

Figure 1: The variance spectrum for the recovery temperature (RTF1, blue line) measured by a Rosemount 102E4AL sensor during a flight segment from the SOCRATES project, flight 15, 6:00:00 – 6:15:00 UTC. The variance spectra for the dynamic-heating term (Q) and for the calculated air temperature after this correction is applied (ATF1) are also shown.

possible by the assumed linearity in response of the sensor, which is required if this part of the response is to be separated from the more general response to the combination of dynamic heating and true fluctuations in temperature.

The revised dynamic-heating adjustment will be labeled Q' to distinguish it from the standard adjustment Q, and the ambient temperature T_a should be estimated from this equation:

$$T_a(t) = T_m(t) - Q'(t) \tag{3}$$

instead of (2). The equation depends on the actual measured (recovery) temperature $T_m(t)$, rather than the true recovery temperature $T_r(t)$ in (2), to emphasize that the measurement is affected by the time-response of the sensor and therefore differs from the true recovery temperature.

This revised adjustment can be obtained by using a numerical solution to the differential equations in Part 1, using only $Q(t)$ as the input term. However, for the high-frequency components numerical integration must be done with considerable attention to accuracy, especially for the unheated Rosemount sensor because its characteristic time constant for the wire response (τ_1) is smaller than the time interval between typically used 25-Hz samples. For this reason, it is preferable to develop an appropriate digital filter having response that matches the transfer function. This also leads to much faster processing.

2.2 A filter for dynamic heating

With the transfer function $H(\omega)$ as determined in Part 1, the impulse response of the sensor can be found from the inverse Fourier transform of that transfer function. Once that is determined, appropriate moving-average coefficients can be found from the impulse response, and those coefficients define a digital filter that represents the sensor response. The procedure used here is somewhat arbitrary, and no claim is made that this is the best filter, but it functions reasonably for 25 Hz measurements. Details including the filter coefficients are provided in Appendix A, and the development of the filter is described in detail in the "Workflow" document (cf. Appendix B) that accompanies this paper.

Figure 2a shows the impulse function for the unheated Rosemount and heated HARCO sensors, and Fig. 2b shows corresponding moving-average coefficients for a filter obtained from this impulse function. There is significant ringing in the filter for the Rosemount sensor because the shorter time constant for the sensor, 0.03 s, is smaller than the time between 25-Hz samples. The impulse response for the slower HARCO sensor leads to a much broader impulse response function. Both sets of moving-average coefficients sum to more than 0.99 as calculated but were then normalized to sum to 1.0.

2.3 Integration, Fourier transformation, and filtering

The response of the sensor to the dynamic-heating signal Q can be found in three ways: integration of the differential equations, Fourier transformation with application of the

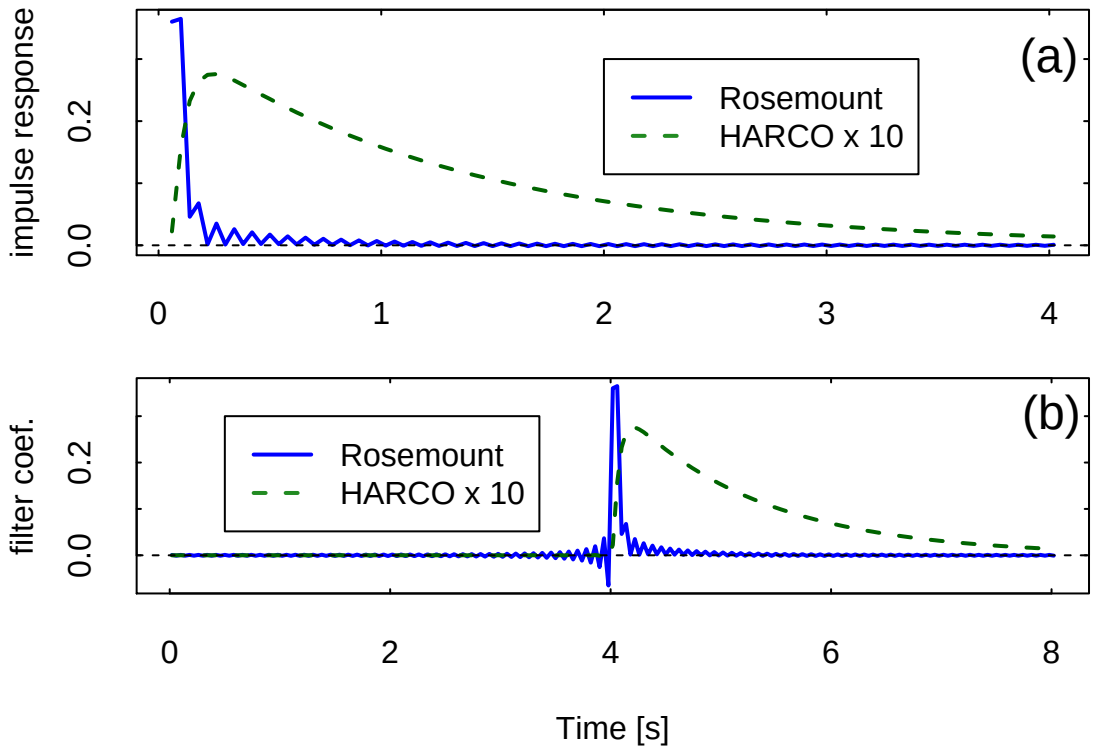

Figure 2: (a) The impulse response function found from the inverse Fourier transform of the transfer function for the unheated Rosemount 102E4AL sensor (Rosemount) and for the heated HARCO sensor (HARCO), using the response parameters from Table 2 of Part 1. The impulse response for the HARCO sensor is multiplied by 10. (b) A filter function (moving-average coefficients spanning 8 s) obtained from the impulse response function. The filtered result must be shifted forward in time by 4 s to compensate for the delay introduced by the filter. The coefficients are multiplied by 10 for the HARCO sensor.

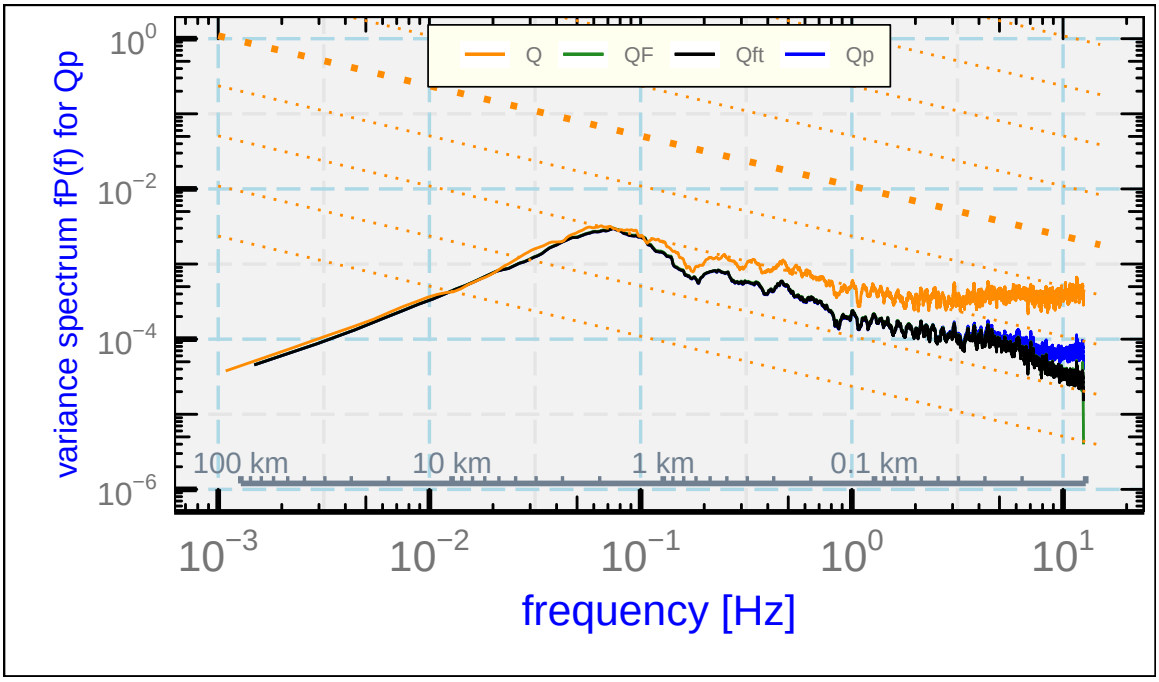

Figure 3: Variance spectra for the dynamic-heating term (Q) and for the filtered term obtained by integrating the differential equations for the derivatives (Qp), by Fourier transformation with application of the transfer function (Qft), or applying the digital filter (QF). The result for the latter is so close to Qft that it is obscured in this plot. Data from SOCRATES flight 15, 6:02:00 to 6:13:00 UTC.

transfer function, or application of the digital filter developed in thepreceding subsection. Those three approaches are explored in this subsection.

With specified differential equations like Part 1 Eqns. (3) and (4), numerical integration can provide estimates of the response of the temperature sensor to the dynamic-heating fluctuations. Applied to dynamic heating, those equations become

$$\frac{dQ_{qs}(t)}{dt} = \frac{Q(t) - Q_{qs}(t)}{\tau_2} \tag{4}$$

$$\frac{dQ'(t)}{dt} = \frac{a(Q(t) - Q'(t)) + (1-a)(Q_{qs}(t) - Q'(t))}{\tau_1} = \frac{\{aQ(t) + (1-a)Q_{qs}(t)\} - Q'(t)}{\tau_1} \tag{5}$$

where the first equation describes the variation of Q_{qs}, the partial response of the support structure to dynamic heating, and the second describes the response of the sensing wire to the combined partial effects of the support temperature as influenced by dynamic heating and the dynamic-heating term. This separation relies on the linearity of the underlying equations, which makes it possible to represent the effect of dynamic heating in isolation from real fluctuations in temperatrure. Euler integration of these differential equations led to erroneous results at high frequency arising from inadequate resolution in the integration, so a fourth-order Runge-Kutta integration[1] was used instead.

[1]The integration method was fourth-order Runge-Kutta with adjustment of the time step to control

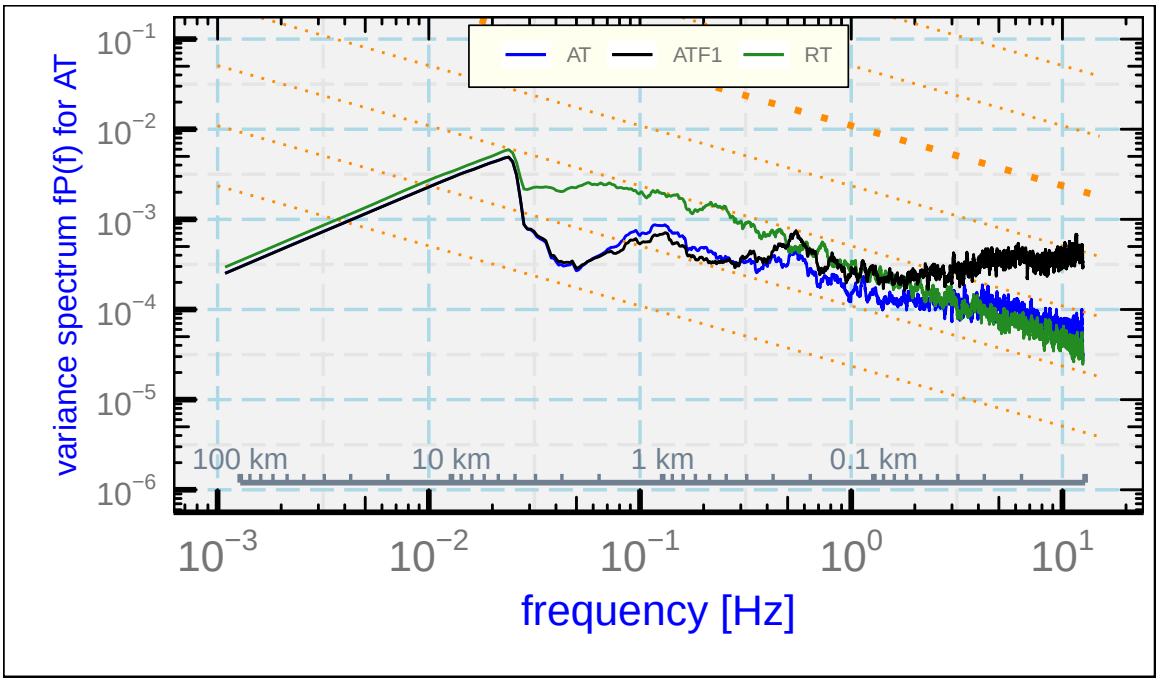

Figure 4: Variance spectra for the measurement of recovery temperature (RT) from the unheated Rosemount 102E4AL sensor and the resulting corrected measurement of ambient temperature (AT) with the filtered dynamic-heating term (QF). The original variable for ambient temperature based on standard processing (ATF1) is also shown. Data from SOCRATES flight 15, 6:00:00 to 6:15:00 UTC.

The response of the sensor is specified by the transfer function, so the filtered response can also be found by first calculating the Fourier transform of the dynamic-heating signal (here denoted $Q^{\dagger}(\nu) = \mathcal{F}(Q(t))$ where $\mathcal{F}$ denotes the Fourier transform) and then using the inverse Fourier transform ($\mathcal{F}^{-1}$) to estimate the sensor response:

$$Q' = \mathcal{F}^{-1}(Q^{\dagger}(\nu)H(\nu))$$

The third option is to apply the digital filter as developed in Sect. 2.2. Appendix A provides more detail.

Figure 3 shows the variance spectra that result from all three methods, applied to measurements from an unheated Rosemount 102E4AL sensor. These results use the same data used in Fig. 1. The modified variance spectrum obtained by integration of the underlying differential equations is shown as the black line ("Qp") in Fig. 3. The dynamic-heating correction is appropriately attenuated at high frequency after this integration. The results obtained after filtering as described in the Sect. 2.2, shown as "QF", or after Fourier transformation, shown as "Qft", are overlapping so as to be indistinguishable in this plot. These corrected estimates of the dynamic heating are attenuated even more than the result from numerical integration and are in better agreement with the predicted effect of the transfer function, which for example predicts attenuation of the variance spectrum by a factor of 0.096 for the component with frequency 10 Hz. The numerical integration was closer to the results of the filter if the measurements are interpolated to 125 Hz with 25-Hz smoothing, integrated, and then resampled to obtain 25 Hz measurements. This illustrated that the discrepancy in results is attributable to accumulating numerical errors in the integration, but the integration became awkwardly slow when performed at 125-Hz resolution. The equivalence of the results from the digital filter and from Fourier transformation with application of the transfer function supports the validity of these results and suggests that these are preferable and equivalent methods for filtering dynamic heating to match the response of the temperature sensor.

With the corrected dynamic-heating term Q', a new estimate of the ambient air temperature was calculated using (3). The spectral variance for air temperature, shown in Fig. 4 as "AT," is improved considerably vs. that using the standard correction ("ATF1"). The new estimate of air temperature is an improved measurement to use in estimates of sensible-heat flux and other studies where the high-rate components of the temperature are important.

In the case of the heated sensors, the revision is still more significant because they respond more slowly. Figure 5 shows the result of filtering the dynamic-heating term with the time constants determined for this sensor. In this case, the result of integration (Qp) and the digital filter (QF) are almost identical so there is no evidence of the integration problems that were encountered with the unheated Rosemount sensor. The effect is quite dramatic even at 1 Hz, and the errors are significant for all frequencies about about 0.1 Hz. Because the variance spectra denoted "QF" or "Qp" represent how the temperature sensor

the estimated tolerance during the integration. The method was based on Cash and Karp [1990]. The integration was also tested with the R routine "rmutil::runge.kutta" Swihart and Lindsey [2019]. See the Workflow document for additional details.

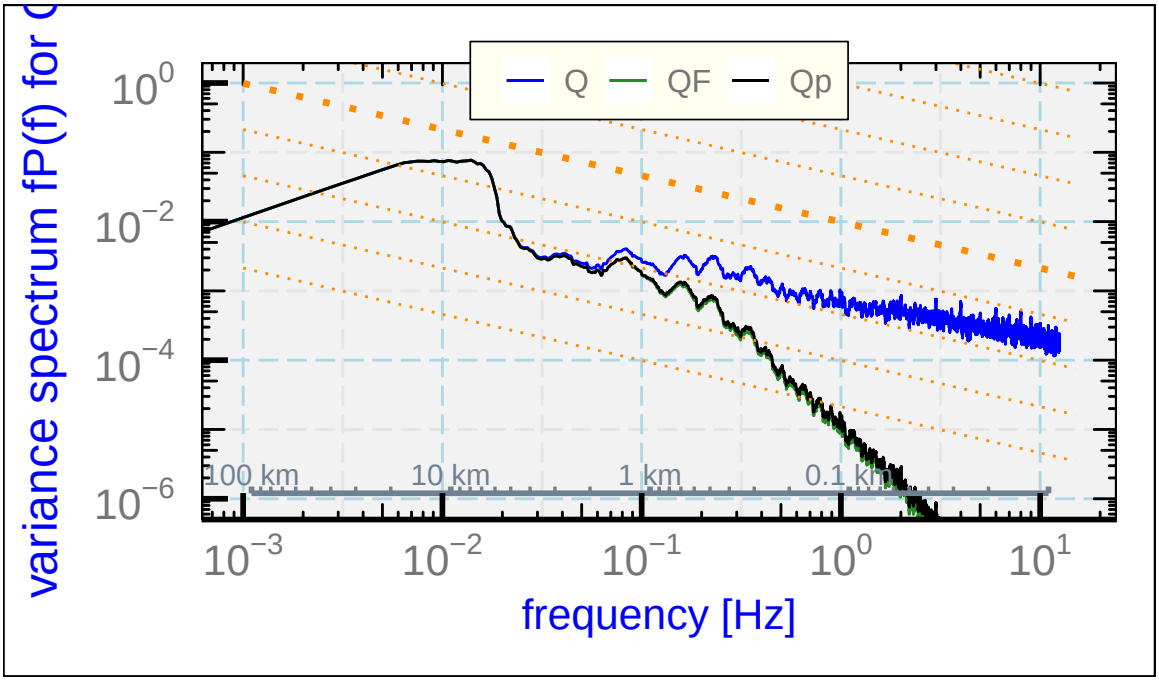

Figure 5: Variance spectra for the unmodified dynamic-heating term and the filtered terms, for measurements from a heated HARCO sensor on the GV research aircraft.

responds to the actual fluctuations, subtracting the actual fluctuations in dynamic heating instead of the filtered fluctuations introduces erroneous variability into the calculated air temperature.

Figure 6 shows how this affects the spectral variance of the measured air temperature from the heated HARCO sensor. The slow response of this sensor causes the measured recovery temperature (RTH1) to have very low spectral variance when the frequency is above 1 Hz, so the variance in the original air-temperature measurement (ATH1) in this frequency range is almost entirely caused by erroneous adjustment for fluctuations in dynamic heating to which the sensor does not respond. The correction procedure leading to Q' removes this excess spectral variance and produces a signal where the variance for frequencies above about 0.1 Hz arises primarily from variance in the measured recovery temperature. The variance spectrum for the conventionally processed temperature looks approximately as might be expected in an inertial subrange, but the variance above about 0.5 Hz is a false signal that does not arise from real variance in temperature. It therefore becomes very important to use this revised processing scheme to avoid erroneous measurements even for changes occurring over 5 s or more.

For the unheated Rosemount 102E4AL sensor, Fig. 7 illustrates the removal of erroneous structure by filtering, and Fig. 8 shows a similar example for the heated HARCO sensor. These plots illustrate that the erroneous fluctuations in the uncorrected measurements can be important in many potential uses of these measurements and should be removed as part of standard processing. The effect is particularly significant for the HARCO sensor, for which there are large fluctuations in Fig. 8 that are caused by fluctuations in dynamic

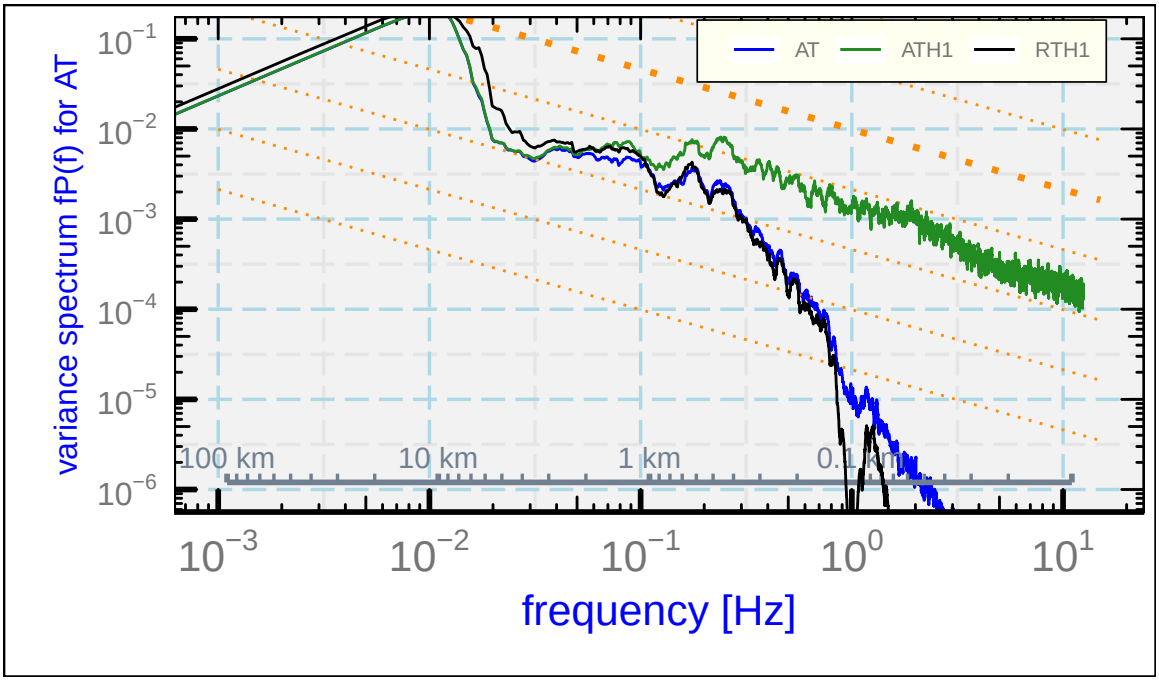

Figure 6: The variance spectra for the original measured temperature and the temperature as modified by filtering the dynamic-heating term for a sample of measurements from a heated HARCO sensor on the GV research aircraft. The plotted spectra are for the measured recovery temperature (RTH1), the conventional calculated air temperature (ATH1), and the revised air temperature (AT) obtained by using the filtered version of the dynamic-heating term (QF).

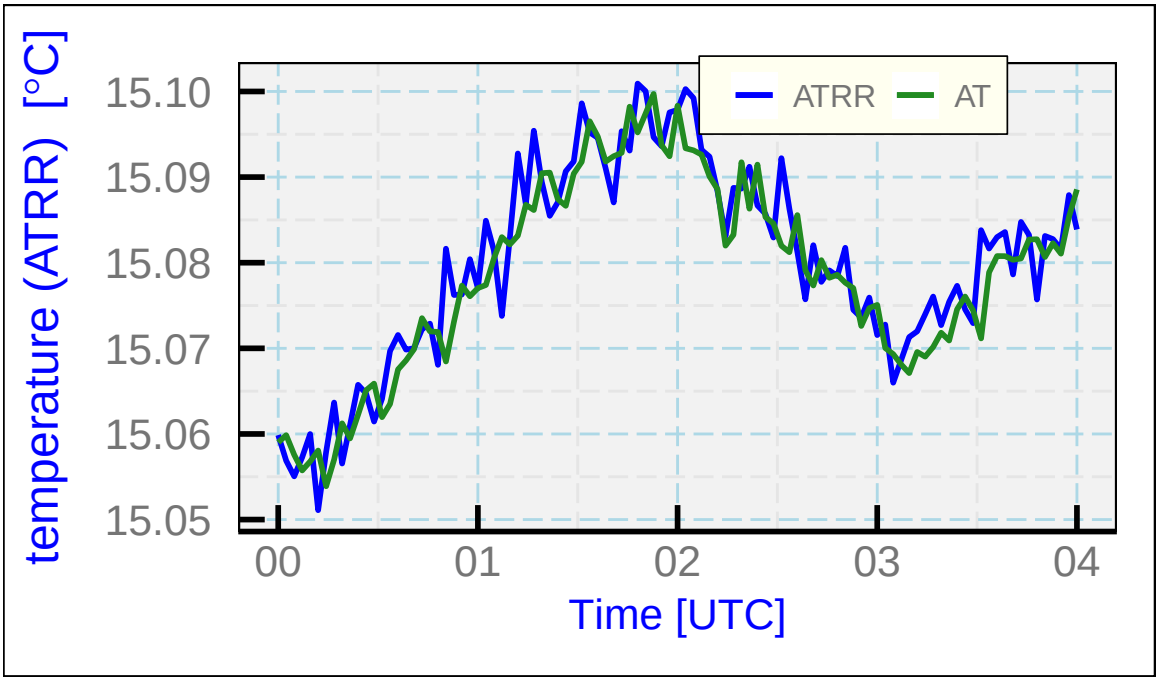

Figure 7: The original measured temperature from an unheated Rosemount 102E4AL sensor (ATRR) and the same temperature after revising the dynamic-heating correction as described in the text (AT). The time is seconds after 8:01:00 UTC for VOCALS flight 3.

heating to which the sensor does not respond, as demonstrated by the corrected measurement of air temperature shown as the green line. Appendix B provides an algorithm and suggested code to implement this correction.[2]

[2]For the NSF/NCAR GV, the dynamic-heating term is complicated further by resonance in the pressure lines connecting the transducers to the pressure sources. This is discussed in detail in Appendix B. That resonance is an additional source of spurious air-temperature noise because the resonance occurs only in the pressure lines and so does not affect the temperature sensor. When they are present, those resonance effects also need to be removed from the dynamic-heating term applied to the recovery temperature.

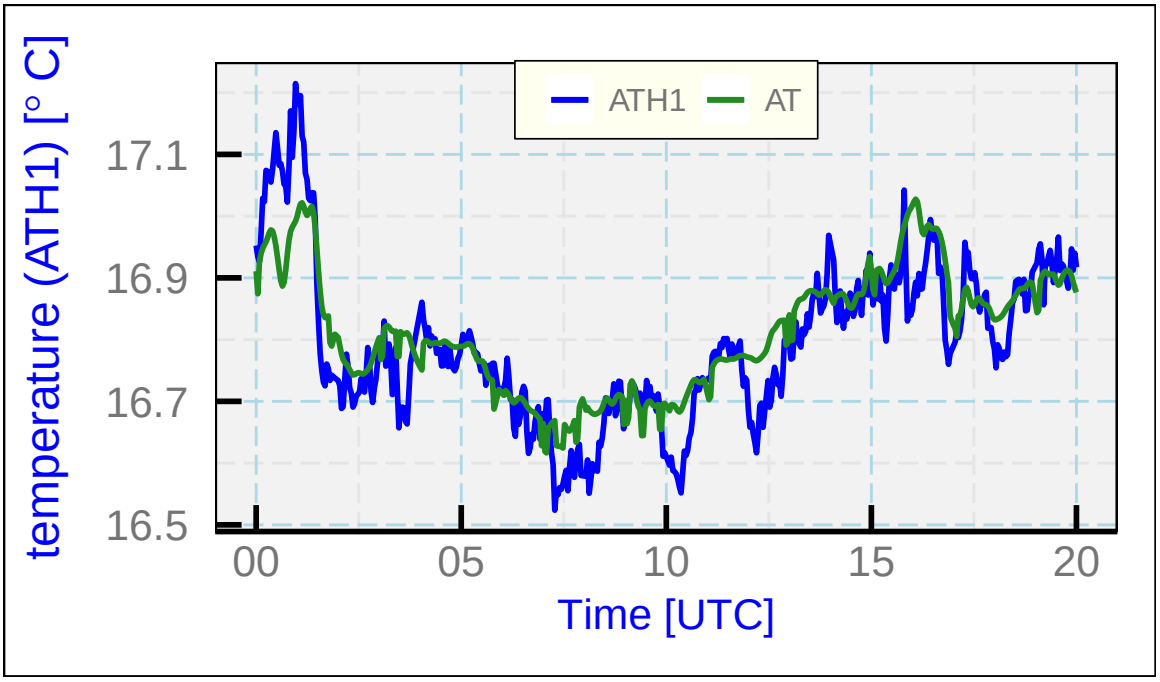

Figure 8: The original measured temperature from a heated HARCO sensor (ATH1) and the same temperature after revising the dynamic-heating correction (AT). The time is seconds after 18:13:00 UTC, for WECAN flight 17.

3 Summary and Conclusions

The primary conclusions of this investigation is that, because standard data processing corrects the measured recovery temperature using an estimate of dynamic heating based on the measured airspeed, such processing often over-corrects and introduces errors because the temperature sensors are not able to respond to the high-frequency fluctuations in measured airspeed. This introduces a significant level of noise into the high-frequency fluctuations in the resulting temperature. A revised treatment of dynamic heating is proposed and shown to lead to improved measurements. A digital filter is presented that can be used to correct standard processing schemes to eliminate the errors arising from the dynamic-heating term.

This Part 2 paper has focused on the dynamic-heating correction needed to obtain the measurement of air temperature from the directly measured recovery temperature. Because the errors discussed here are so prevalent in almost all existing data from research aircraft, it is essential to be able to remove these errors, and this paper develops one way of correcting these errors. Part III will then turn to the implications for measuring the flux of sensible heat.

A The Digital Filter for Dynamic Heating

As described in Sect (2.2), digital filters for dynamic heating were developed from the transfer functions for the probes studied in Part 1. The procedure was to use the inverse Fourier transforms of those transfer functions, which give the impulse response functions, and then design filters using coefficients determined from those impulse functions. This appendix describes in more detail how this was done and includes references to the coefficients that might be used by others. The filters so obtained appear to function as desired, although this is an area where further work will be warranted.

The procedures was as follows:

1. Use the response parameters for the sensor (e.g., for the unheated Rosemount 102E4AL sensor or the heated HARCO sensor) and a large set of frequencies spanning the interval from -12.5 to 12.5 Hz, e.g., with resolution between assumed frequencies of $(1/600)$ Hz, in the solution specified by Part 1 Eqs. (7) and (8) to specify the transfer function. This solution is stored in a vector with frequencies in the order (0 to 12.5 Hz, then $(-12.5 + 1/600)$ to $-(1/600)$ Hz, as is conventional for representations of the Fourier transform in R and also many other languages. It was essential to calculate the negative-frequency components and, to obtain real-number results, to store then is that the values representing negative frequencies are the complex conjugates of those for the corresponding positive frequencies.

2. The inverse Fourier transform then gave the impulse function at 15,000 delays, many of them representing negative delays. The values in the central part of this array were mostly very small.

3. To obtain a manageable number of moving-average coefficients, all values in the array representing the impulse function were set to zero for indices k with values $M + 2 \leq k \leq N - M$ where N is the length of the calculated impulse function and $M = 100$ to leave 201 non-zero coefficients. This gave coefficients spanning about 8 s at 25 Hz, or a time long compared to the expected impulse response of the sensor.

4. The upper-100 coefficients represent negative delays in the impulse response because of the cyclic nature of the Fourier transform, so the coefficients were re-arranged into a sequence with the last-100 coefficients first and the initial-101 coefficients moved to the end of the array. These coefficients were then moving-average coefficients that implement a filter matching the transfer function, except for some omitted terms outside the 200-coefficient range that are assumed negligible.

5. The resulting set of moving-average coefficients can then be applied to the measured dynamic-heating term Q to produce a filtered version.

6. The filtered result then needs to be shifted in time by 4 s to correct for the offset in the filter.

As an illustration, R code to define filter coefficients for use with 25-Hz samples is listed here for the unheated Rosemount 102E4AL sensor:

```
NP <- 15000  ## Assume 10-min segment
df <- 25 / NP
frq <- c(seq(0, 12.5, by=df), seq(-12.5+df, -df, by=df))
E <- LTphase(frq, P)  ## This function returns the gain and phase in deg.
G <- complex(modulus=E$Amp, argument=E$Phase * pi / 180) # the transfer fn
NG <- length(G)
GT <- fft(G, inverse=TRUE) / NG  # get the impulse function
## Limit to 200 coefficients (8 s at 25 Hz)
Lshift <- 100  ## below, will need to shift by 100 40-ms samples
GT[(Lshift + 2):(NP - Lshift)] <- complex(modulus=0)
GTT <- GT[GT != complex(modulus=0)]
## Reorder:
GTT <- c(GTT[(Lshift + 2):length(GTT)], GTT[1:(Lshift + 1)])
AR <- Arma(Re(GTT) / sum(Re(GTT)), 1) # Normalize to avoid <1% bias
## Result is appropriate coefficients to use for filtering;
## e.g., if DF is data.frame with Q measured dynamic heating:
DF$QF <- as.vector(signal::filter(AR, DF$Q)) ## standard R
## the following is a function to shift in time:
DF$QF <- ShiftInTime(DF$QF, .shift=-Lshift * 40, .rate=25)
```

The 201 coefficients in "AR" are archived in the zip file included in the GitHub repository for this project, as described in Appendix C. Other autoregressive moving-average (ARMA) coefficients included there, which can be used as in the last three code lines above, are listed in the following table:

sensor	**aircraft**	**data rate [Hz]**	**ARMA**	**time shift [s]**
unheated Rosemount 102E4AL	C-130	25	AR	4
"	"	1	AR1	10
"	GV	25	ARG	4
"	"	1	ARG1	10
heated HARCO	both	25	AH	6
"	"	1	AH1	10

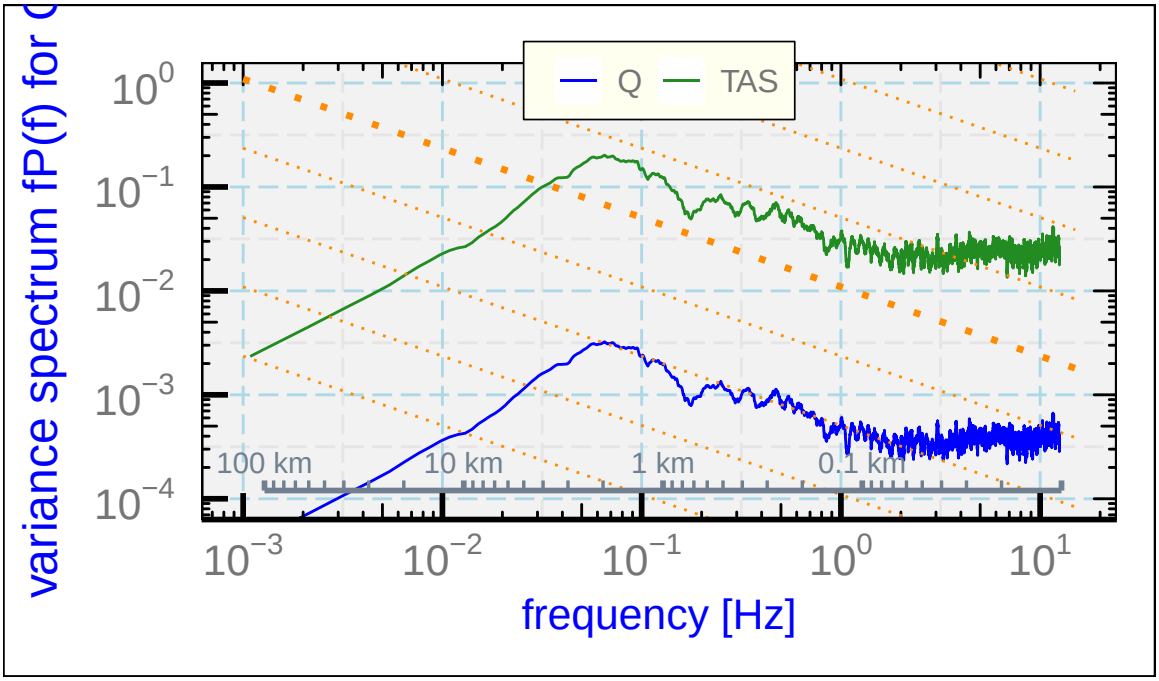

Figure 9: The variance spectrum for the dynamic-heating correction Q, from SOCRATES flight 15, 6:00:00 to 6:15:00 UTC, in a region thought to have characteristics of an inertial subrange. The variance spectrum for the airspeed measurement (TASX) is also shown.

B Pressure-Line Resonance

Cooper et al. [2016] showed evidence that the variance spectrum of the longitudinal component of the wind appears to have excess variance at frequencies above about 2 Hz. Figure 9 shows the problem: Both the airspeed and the dynamic heating calculated from it have excess variance above the expected distribution for frequencies above about 2 Hz, although this is a turbulent region with characteristics otherwise consistent with an inertial subrange. The lateral components of the wind do not show this excess variance; it only appears in the longitudinal component. It is far above the noise expected from the precision of the sensor used to measure the dynamic pressure (estimated at about 0.1 hPa), so there must be another source of this contamination of the signal. The suggested explanation (by D. Lenschow, included in that same reference, p. 140) is that there is resonance in the long lines connecting the pressure ports to the pressure transducers and that causes either amplification or attenuation of the pressure signals, along with phase shifts, at various frequencies. If this extraneous variance arises in the pressure lines, it does not influence the temperature sensor so subtraction of the measured dynamic-heating term from the recovery temperature to obtain the ambient temperature introduces still more high-frequency noise into the measurement of air temperature. When correcting for temperature-sensor time response, this additional source of false variation in the dynamic-heating term should be removed where possible. This appendix discusses a possible approach to that removal.

The argument presented in Cooper et al. [2016] was that line resonance in the static

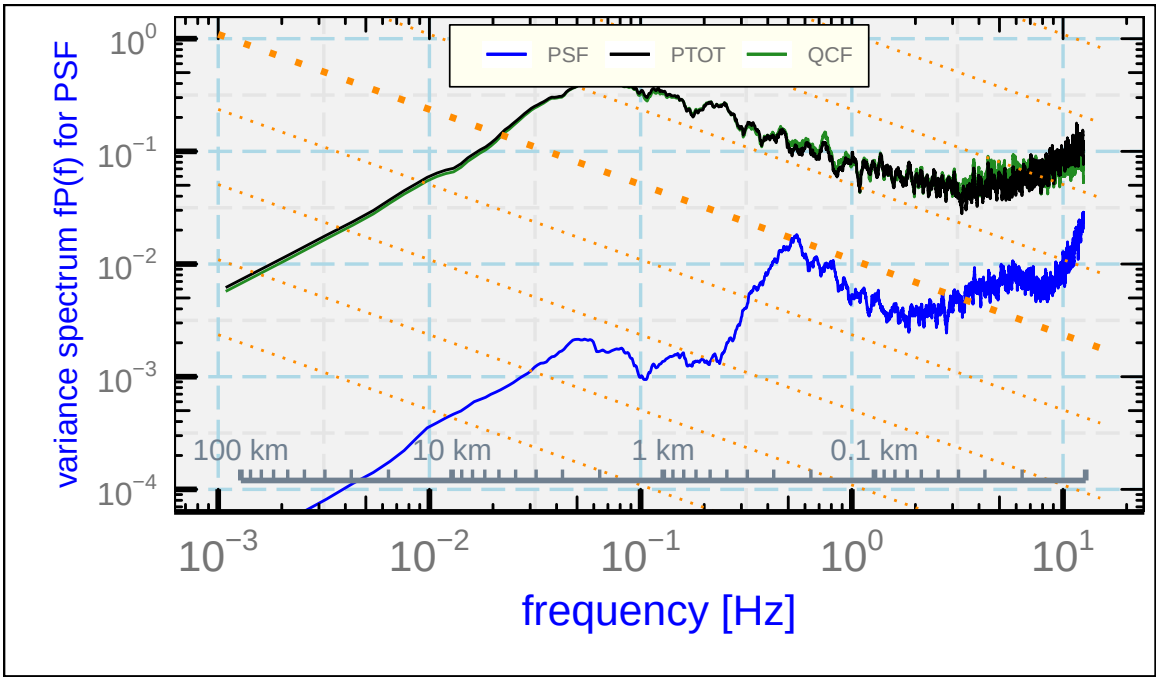

Figure 10: Variance spectra for three pressure measurements: the ambient or static pressure (PSF), the dynamic pressure (QCF), and their sum (PTOT).

pressure line used as a lower-pressure reference for the dynamic-pressure measurement was responsible. It appears now that this was not the correct explanation. The reason is that fluctuations in static pressure normally make a negligible contribution to the measured fluctuations in dynamic pressure; instead, fluctuations in dynamic pressure are dominated by fluctuations in the total pressure delivered by the pitot tube to the differential sensor. Figure 10 shows that the dominant contributions to variance in dynamic pressure, measured as the difference between the total and static pressure, comes from the variance in the total pressure present in the shorter inlet line. Resonances in both lines need to be evaluated, but the following argument indicates that the fluctuations in the static-pressure line do not make any significant contribution to fluctuations in measured dynamic pressure.

Lenschow's analysis (based on theoretical predictions of Iberall [1950]) leads to a transfer function representing the effect of the line resonance on the measurement. This transfer function was plotted in Fig. 52 of Cooper et al. [2016] and has been recalculated from the equations in Iberall [1950], specifically Eqs. (105) and (106) with (99) and (95) and with the volume within the pressure sensor at the end of the line assumed to be 300 mm^3 as used by D. Lenschow, for use in the present work. That transfer function then can be used in the same way as the time-response transfer function to correct the measured dynamic-heating term by applying the correction to both lines connected to the dynamic-pressure sensor. The result should be a better estimate of the dynamic heating at the temperature sensor because the fluctuations occurring only in the lines and not affecting the temperature sensor will be removed.

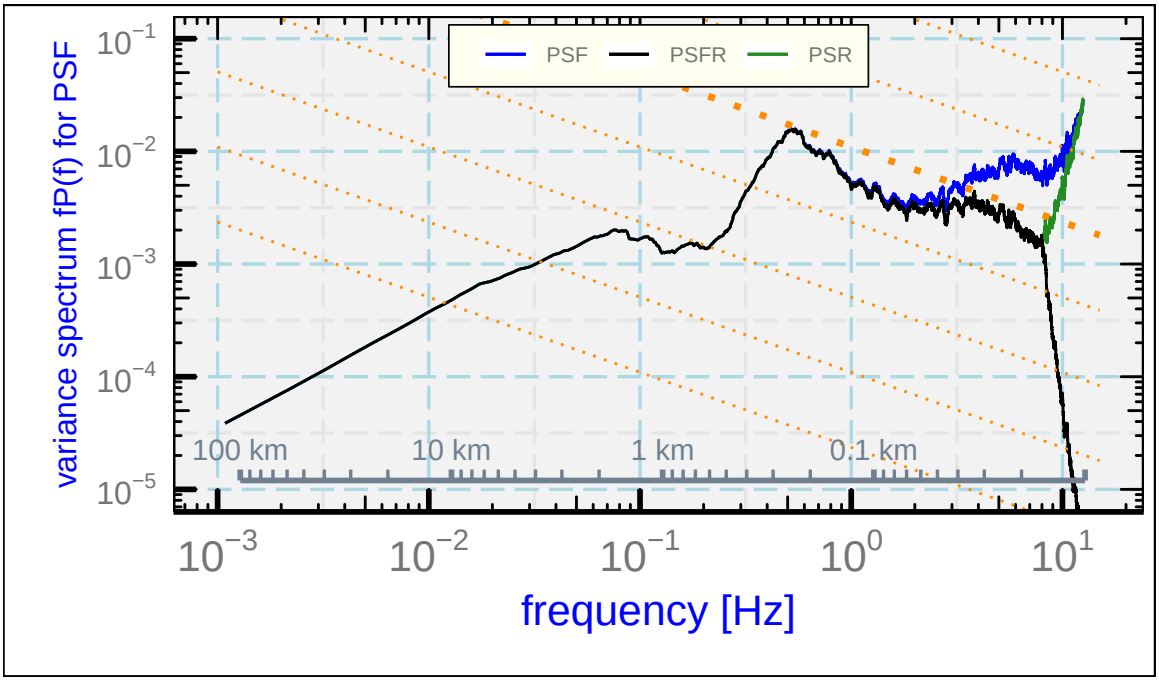

Figure 11: The variance spectrum that results from correcting the measured static pressure ("PSF") for the theoretical effect of line resonance, represented here as "PSR". To reduce suspected noise, additional attenuation is applied above 8 Hz to obtain "PSFR".

Consider first the effect on static pressure. The predicted transfer function is based on a theoretical analysis, so it is useful to determine if the correction based on that transfer function is reasonable. In a region thought to represent an inertial subrange, the slope of the variance spectrum of the longitudinal wind (and therefore of airspeed fluctuations at high frequency and also the dynamic-heating term) is expected to exhibit a $-5/3$ slope with frequency or a $-2/3$ slope in the frequency-weighted spectral-variance plots used here. Measurements of static pressure from the same region shown in Figs. 9 and 10 were processed by calculating the Fourier transform of the pressure, dividing by the transfer function, and using an inverse Fourier transform to recover the corrected pressure. The result is shown as "PSR" in Fig. 11, as the green line (mostly overlapped at low frequency by the black line). The result seems reasonable for frequencies below about 8 Hz, but there is a sharp increase above that point. Two possible causes are: (i) The sensor resolution, thought to be 0.1 hPa from the manufacturer's specified uncertainty limit, would cause a noise spectrum of about this magnitude, although with a smaller slope; and (ii) aliasing of higher-frequency fluctuations may contribute. The digital filters applied to the measurements don't remove this aliasing because the fluctuations are real fluctuations in pressure in the pressure lines and so will still be sampled as aliased. For these reasons, additional filtering was applied to the Fourier components before inverse transformation to reduce frequencies above 8 Hz. The result, shown as "PSFR" in the figure, is a reasonable adjustment to the original variance spectrum to account for line resonance for frequencies below 8 Hz, and evidently excess variance at higher frequency has been removed

This approximate agreement between predictions for the measured static pressure and the expected shape of the variance spectrum after correction, for frequency below 8 Hz, provides some support for the theoretical analysis by greatly improving the appearance of the variance spectrum for pressure, although the shape is still not ideal. The spectrum would appear better if the gain of the transfer function around 4 Hz were approximately 40% larger so that the variance there would be reduced by about a factor of 2. Although the distance from the static source to the pressure transducer is only about 3 m, it appears that resonance in the branch of this line that continues forward to the differential transducer affects the signal also at this location.

Analysis of the effect of line resonance on the measurement of dynamic pressure is more complicated because resonance can occur in both lines, the line delivering total pressure from the pitot tube and the line delivering static pressure from the static sources. The measured quantity at the differential pressure transducer is the difference between the total-pressure-line resonating pressure and the ambient-pressure-line resonating pressure, so (using primes to denote quantities in the resonating lines) $p'_t = q' + p'_s$ is the true total pressure in the line from the pitot tube. This can be corrected using the theoretical transfer function for that line[3] to obtain the true total pressure at the inlet to the pitot tube, p_t, and then the best estimate of the true dynamic pressure q is $q = p_t - p_s$ where corrected quantities are used for both p_t and p_s, the latter as estimated from "PSFR" in Fig. 11.

It is notable that the variance spectrum for the measured static pressure, "PSF", is far below that for the corrected dynamic pressure ("QCFR") or for the original measurement ("QCF"), except near 12 Hz. That confirms that resonance in the long line supplying static pressure to the differential pressure sensor has little effect on the measurement of dynamic pressure and hence on the measurement of the longitudinal component of the wind. The important contribution appears to be from resonance in the total-pressure line.

This correction greatly improves the variance spectrum for dynamic pressure by giving a slope consistent with expectations for an inertial subrange. During this flight segment, other measurements (notably the vertical wind) indicate $-5/3$ slope, while the uncorrected measurement (QCF) departs from that slope significantly for frequencies above about 4 Hz. The excess variance present at these frequencies therefore should also be removed from estimates of dynamic heating based on dynamic pressure, before the filtering to account for temperature-sensor response (Sect. (2.2)) is applied.

[3]Assumed parameters are length 4 m, diameter 3.1 mm, sensor volume $10^4\,\mathrm{mm}^3$. These need confirmation and possible adjustment. They were selected primarily to produce the appropriately corrected variance spectrum for dynamic heating. The sensor volume in particular is probably too high.

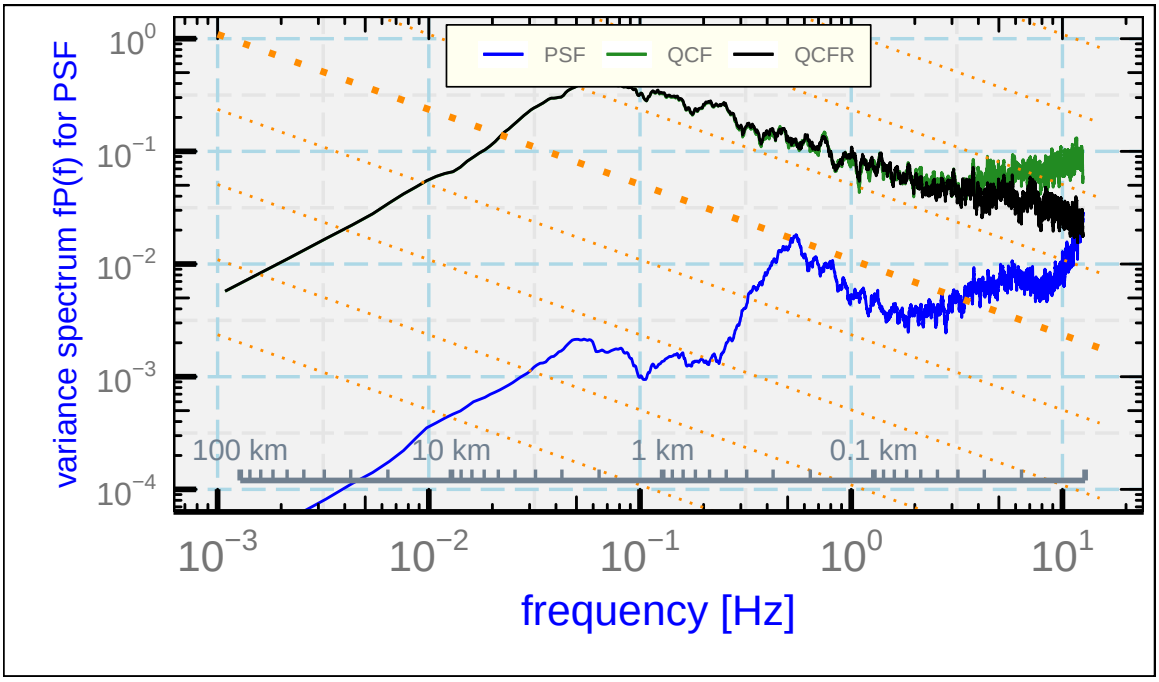

Figure 12: Variance spectra for the best estimate for dynamic heating, "QCFR", after correction for resonance in both lines connected to the differential pressure sensor that produces the original measurement "QCF". The corresponding spectrum for the measured pressure in the line connected to the static sources ("PSF") is also shown.

C Reproducibility

This document is constructed in ways that support duplication of the study. The code that generates the plots and implements the correction procedure is incorporated into the same file that generated this document via LaTeX, using principles and techniques described by Xie [2013] as implemented in the R package 'knitr' (Xie [2014]). The program, 'SensibleHeatFluxPaper1.Rnw', is archived on 'GitHub' in the directory at this URL. There is some supplemental material in that directory, including the workflow document, the bibliography and some code segments saved in the "chunks" subdirectory, so the full directory should be downloaded in order to run the program. The calculations use the programming language R (R Core Team [2019]) and were run within RStudio (RStudio [2009]), so this is the most straightforward way to replicate the calculations and the generation of this document.

A package named Ranadu, containing auxillary functions, is used extensively in the R code. It is available on GitHub as https://github.com/WilliamCooper/Ranadu.git. The version used for calculations in this technical note is included in the 'zip' archive listed below.

The data files used are also preserved in the NCAR/EOL Data Archives and can be obtained via a request to `mailto:raf-dm@eol.ucar.edu` or via the "Data Access" links at this web site. The original files containing the data as produced by the NCAR Earth Ob-

serving Laboratory, Research Aviation Facility, were in netCDF format (cf. this URL), but in many cases data archives were reprocessed and the files may change after reprocessing so a separate archive is maintained for this document. The data files in this archive contain R data.frames and are preserved as binary-format 'Rdata' files via R 'save' commands. The code in the GitHub archive has appropriate 'load' commands to read these data files from a subdirectory named 'Data' (/Data or ~/Data or /home/Data) but this is not part of the GitHub repository because it is too large to be appropriate there. To reproduce this research, those data files have to be transferred separately from {??where??}

Extensive use has been made of attributes assigned to the data.frames and the variables in those data.frames. All the attributes from the original netCDF files have been transferred, so there is a record of how the original data were processed, for example recording calibration coefficients and processing chains for the variables. Once the data.frames are loaded into R, these attributes can be viewed and provide additional documentation of what data were used. Key information like the processing date, the program version that produced the archive, and the selection of primary variables for various measurements thus is preserved.

(See the related list of project components on the next page that are preserved to enhance reproducibility.)

PROJECT:	SensibleHeatFlux
ARCHIVE PACKAGE:	SensibleHeatFluxPaper2.zip
CONTAINS:	attachment list below
PROGRAM:	SensibleHeatFluxPaper2.Rnw
ORIGINAL DATA:	UCAR/NCAR - Earth Observing Laboratory [2011], UCAR/NCAR - Earth Observing Laboratory [2019], UCAR/NCAR - Earth Observing Laboratory [2017]
SPECIAL DATA FILES:	SensibleHeatFlux.Rdata, SensibleHeatFluxPaper2.Rdata, AR.Rdata
WORKFLOW DOCUMENT:	WorkflowSensibleHeatFluxPaper2.pdf
GIT:	https://github.com/WilliamCooper/SensibleHeatFlux.git

Attachments:
SensibleHeatFluxPaper2.Rnw
SensibleHeatFluxPaper2.pdf
WorkflowSensibleHeatFluxPaper2.pdf
WAC.bib
chunks/*
SessionInfo

References

Jens Bange, Marco Esposito, Donald H. Lenschow, Philip R. A. Brown, Volker Dreiling, Andreas Giez, Larry Mahrt, Szymon P. Malinowski, Alfred R. Rodi, Raymond A. Shaw, Holger Siebert, Herman Smit, and Martin Zöger. *Measurement of Aircraft State and Thermodynamic and Dynamic Variables*, chapter 2, pages 7–75. John Wiley & Sons, Ltd, 2013. ISBN 9783527653218. doi: 10.1002/9783527653218.ch2. URL https://onlinelibrary.wiley.com/doi/abs/10.1002/9783527653218.ch2. 2

Jeff R Cash and Alan H Karp. A variable order runge-kutta method for initial value problems with rapidly varying right-hand sides. *ACM Transactions on Mathematical Software (TOMS)*, 16(3):201–222, 1990. 1

W. A. Cooper, R. B. Friesen, M. Hayman, J. B. Jensen, D. H. Lenschow, P. A. Romashkin, A. J. Schanot, S. M. Spuler, J. L. Stith, and C. Wolff. Characterization of uncertainty in measurements of wind from the NSF/NCAR Gulfstream V research aircraft. NCAR technical note NCAR/TN-528+STR, Earth Observing Laboratory, NCAR, Boulder, CO, USA, jul 2016. URL http://n2t.net/ark:/85065/d7qr4zqr. B, B, B

Berend Hasselman. *nleqslv: Solve Systems of Nonlinear Equations*, 2018. URL https://CRAN.R-project.org/package=nleqslv. R package version 3.3.2. (document)

A. S. Iberall. *J. Res. Natn. Bur. Stand.*, (45):85–108, 1950. doi: 10.6028/jres.045.008. URL http://nvlpubs.nist.gov/nistpubs/jres/045/jresv45n1p85_A1b.pdf. B

David Pierce. *ncdf4: Interface to Unidata netCDF (Version 4 or Earlier) Format Data Files*, 2015. URL https://CRAN.R-project.org/package=ncdf4. R package version 1.15. (document)

R Core Team. *R: A language and environment for statistical computing*. R Foundation for Statistical Computing, Vienna, Austria, 2019. URL http://www.R-project.org. (document), C

RStudio. *RStudio: Integrated development environment for R (Version 0.98.879)*, 2009. URL http://www.rstudio.org. (document), C

Bruce Swihart and Jim Lindsey. *rmutil: Utilities for Nonlinear Regression and Repeated Measurements Models*, 2019. URL https://CRAN.R-project.org/package=rmutil. R package version 1.1.3. (document), 1

UCAR/NCAR - Earth Observing Laboratory. NCAR/NSF C-130 navigation, state parameter, and microphysics HRT (25 sps) data. version 1.0 [data set, VOCALS], 2011. URL https://doi.org/10.5065/d69k48jk,Accessed09Jan2020. (document), C

UCAR/NCAR - Earth Observing Laboratory. High rate (hrt - 25 sps) navigation, state parameter, and microphysics flight-level data. version 2.0. [data set, CSET], 2017. URL https://doi.org/10.5065/D63R0R3W,Accessed12Mar2020. C

UCAR/NCAR - Earth Observing Laboratory. High rate (HRT - 25 sps) navigation, state parameter, and microphysics flight-level data. version 0.1 [preliminary] [data set, WE-CAN], 2018. URL https://data.eol.ucar.edu/dataset/548.004. Accessed09Jan2020. (document)

UCAR/NCAR - Earth Observing Laboratory. High rate (HRT) navigation, state parameter, and microphysics flight level data. version 1.0 [data set, SOCRATES], 2019. URL https://doi.org/10.26023/K5VQ-K6KY-W610,Accessed09Jan2020. (document), C

H. Wickham. *ggplot2: elegant graphics for data analysis*. Springer New York, 2009. ISBN 978-0-387-98140-6. URL http://had.co.nz/ggplot2/book. (document)

Y. Xie. *Dynamic Documents with R and knitr*. Chapman and Hall/CRC, Boca Raton, Florida, 2013. URL http://yihui.name/knitr/. ISBN 978-1482203530. (document), C

Y. Xie. *knitr: A general-purpose package for dynamic report generation in R*, 2014. URL http://yihui.name/knitr/. R package version 1.6. (document), C